

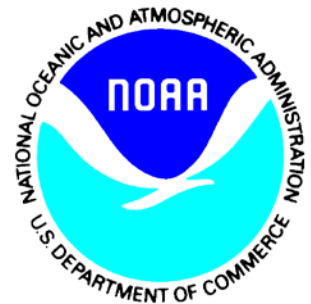
---

**Snowfall Rate (SFR)**

# **Algorithm Theoretical Basis Document**

*Compiled by the*

**SFR Integrated Product Team (IPT),  
MiRS IPT,  
Office of Satellite and Product Operations (OSPO),  
and NOAA Data Exploitation (NDE) Project**



**Version 1.1**  
**May, 2019**

---

TITLE: SNOWFALL RATE (SFR) ALGORITHM THEORETICAL BASIS DOCUMENT

AUTHORS:

Huan Meng (NOAA NESDIS/STAR)  
Ralph Ferraro (NOAA NESDIS/STAR)  
Jun Dong (U. Maryland/ESSIC/CICS-MD)  
Cezar Kongoli (U. Maryland/ESSIC/CICS-MD)  
Limin Zhao (NOAA NESDIS/OSPO)  
Quanhua Liu (NOAA NESDIS/STAR)  
Christopher Grassotti (U. Maryland/ESSIC/CICS-MD)  
Shuyan Liu (CIRA)

**DOCUMENT HISTORY  
 DOCUMENT REVISION LOG**

The Document Revision Log identifies the series of revisions to this document since the baseline release. Please refer to the above page for version number information.

<b>DOCUMENT TITLE: Algorithm Theoretical Basis Document</b>			
<b>DOCUMENT CHANGE HISTORY</b>			
<b>Revision No.</b>	<b>Date</b>	<b>Revision Originator Project Group</b>	<b>CCR Approval # and Date</b>
1.0	June 2018	Version 1.0	N/A
1.1	May 2019	Version 1.1	N/A



## TABLE OF CONTENTS

	<u>Page</u>
LIST OF TABLES AND FIGURES.....	6
1. INTRODUCTION .....	7
1.1. Product Overview .....	7
1.1.1. Product Description .....	7
1.1.2. Product Requirements .....	7
1.2. Satellite Instrument Description .....	8
2. ALGORITHM DESCRIPTION .....	9
2.1. Processing Outline .....	9
2.2. Algorithm Input.....	12
2.3. Theoretical Description.....	14
2.3.1. Physical Description .....	14
2.3.2. Mathematical Description .....	16
2.4. Algorithm Output.....	19
2.5. Performance Estimates .....	20
2.5.1. Test Data Description.....	20
2.5.2. Sensor Effects .....	20
2.5.3. Retrieval Errors.....	21
2.6. Practical Considerations .....	24
2.6.1. Numerical Computation Considerations.....	24
2.6.2. Programming and Procedural Considerations .....	25
2.6.3. Quality Assessment and Diagnostics .....	25
2.6.4. Exception Handling.....	25
2.7. Validation .....	26
3. ASSUMPTIONS AND LIMITATIONS.....	27
3.1. Performance Assumptions.....	27
3.2. Potential Improvements.....	28
1. REFERENCES.....	30

**LIST OF TABLES AND FIGURES**

	<u>Page</u>
Table 1-1. JPSS ATMS SFR Latency Requirements .....	8
Table 1-2. JPSS ATMS SFR Requirements .....	8
Table 2-1. Over-Land SD Validation Metrics .....	22
Table 2-2. Over-Land SFR Validation Metrics against Stave IV over CONUS .....	22
Table 2-3. Over-Land SFR Validation Metrics against MRMS over CONUS.....	23
Table 2-4. ATMS SFR Error Budget.....	24
Figure 2-1. Diagram showing SFR processing as a sub-system within MiRS .....	9
Figure 2-2. SFR processing flowchart .....	10
Figure 2-3. Diagram of inversion processing (1DVAR) to retrieve cloud properties for deriving SFR .....	12
Figure 2-4. Impact of cloud ice and rain in simulated brightness temperatures in the range 1 to 330 GHz. The shaded area indicates the spectral range of the ATMS channels. ....	15
Figure 2-5. SFR change corresponding to TB perturbation at 165.5 GHz and 183.31±7 GHz .....	21
Figure 2-6. S-NPP ATMS SFR validation against Stage IV; left: scatter plot, right: probability distribution.....	22
Figure 2-7. S-NPP ATMS SFR validation against Stage IV; left: scatter plot, right: probability distribution.....	23

## 1. INTRODUCTION

### 1.1. Product Overview

#### 1.1.1. Product Description

Product description with sufficient detail so that the user understands how to use the product files. (*Document Object 34*)<sup>1</sup>

**Writers:** Algorithm Scientists.

The ATMS SFR product is the instantaneous liquid-equivalent snowfall rate. The current algorithm is only applicable over global land although the requirement is global (land and ocean). The SFR product is retrieved from measurements taken by passive microwave sensors aboard certain polar-orbiting satellites. It is composed of two algorithms: snowfall detection and rate estimation. Both algorithms have been validated before SFR for a specific satellite is transitioned to operation.

Operationally, this product is generated inside the NOAA Microwave Retrieval Integrated System (MiRS). Even though the SFR algorithm is independent of MiRS, they share the same input, and the SFR product is generated from the MiRS processing and included in the MiRS output files.

#### 1.1.2. Product Requirements

State the requirements for each product, either explicitly or by reference to the project's requirements document, if available. Product requirements should include content, format, latency, quality. (*Document Object 1*)

**Writers:** Development Lead.

The AMSU/MHS SFR product went into operation at NOAA/NESDIS in 2012. Four satellites carry the sensor pair: NOAA-18, NOAA-19, Metop-A, and Metop-B. ATMS SFR was added to the JPSS Baseline Requirement Documents (L1RD) in 2018. This allows the S-NPP and JPSS SFR to be transitioned to operation. Table 1-1 lists the JPSS latency requirements for ATMS SFR. Table 1-2 shows other JPSS L1RD requirements.

The SFR product is distributed in the MiRS imaging products file (IMG) in the netCDF4 format. Besides snowfall rate including no snowfall, the product also includes flags indicating the conditions for no-retrieval.

---

<sup>1</sup> If Document Objects have been written, the indicated object should be directly inserted to satisfy each template instruction. Document Objects are described in the Algorithm Theoretical Basis Document Standards and Guidelines [http://projects.osd.noaa.gov/spsrb/standards\\_data\\_mtg.htm](http://projects.osd.noaa.gov/spsrb/standards_data_mtg.htm)

Table 1-1. JPSS ATMS SFR Latency Requirements

Product/Parameter	Maximum Latency (minutes)		Data Recipients						
	Total System (Th./Obj.) (1)	Allocated To Entity (Threshold)	JPSS GS – ESPC	JPSS GS – CLASS	JPSS GS – USN	ESPC – NOAA	ESPC – CLASS (10)	ESPC – AFWA (9)	ESPC – USN (9)
ATMS Snowfall Rate	96/30								
JPSS Ground System CRIS/ATMS SDR (4)		114	X						
ESPC Product Generation (3)		16				X	X	X	X

Table 1-2. JPSS ATMS SFR Requirements

EDR Attribute	Threshold	Objective
<b>Snowfall Rate Applicable Conditions:</b> Limb-corrected 53.6 GHz $\geq$ 240 K		
<b>Geographic Coverage</b>	Global land	Global
<b>Vertical Coverage</b>	Single layer in lower atmosphere	Single layer in lower atmosphere
<b>Horizontal Cell Size</b>	15 km at nadir	15 km at nadir
<b>Mapping Uncertainty, 3 Sigma</b>	N/A (reflects SDR characteristics)	N/A (reflects SDR characteristics)
<b>Measurement Range</b>	N/A	N/A
<b>Snowfall Rate Accuracy</b>	0.3 mm/hr	0.15 mm/hr
<b>Snowfall Rate Precision</b>	1 mm/hr	0.7 mm/hr
<b>Probability of Detection</b>	40% over land and 30% over ocean	50% over land and 40% over ocean
<b>False Alarm Rate</b>	15% over both land and ocean	10% over both land and ocean
<b>Refresh</b>	Twice Daily	Twice Daily

The SFR latency requirements are met since SFR is part of the MiRS processing and the latter meets the same latency requirements. Other SFR attributes are discussed throughout this document especially in Section A5.2.3.

## 1.2. Satellite Instrument Description

Describe the attributes of the sensing system(s) used to supply data for the retrieval algorithm at a level of detail sufficient for reviewers to verify that the instrument is capable of supplying input data of sufficient quality. (*Document Object 28*)

**Writers:** Development Lead and PAL should collaborate.

The SFR product is derived from the AMSU/MHS and ATMS sensors. Refer to MiRS ATBD Section 1.2 for descriptions of these instruments.

## 2. ALGORITHM DESCRIPTION

### 2.1. Processing Outline

Full description of the processing outline of the retrieval algorithm. All key elements and sub-elements needed to convey a comprehensive sense of the algorithm should be included. The level of detail should be consistent with the current maturity of the software architecture (which will improve with each revision). A data flow diagram consistent with the software architecture is preferred. *(Document Object 13)*

**Writers:** Algorithm Scientists.

The SFR product is generated inside the MiRS system. Figure 2-1 presents the SFR processing as a sub-system within MiRS.

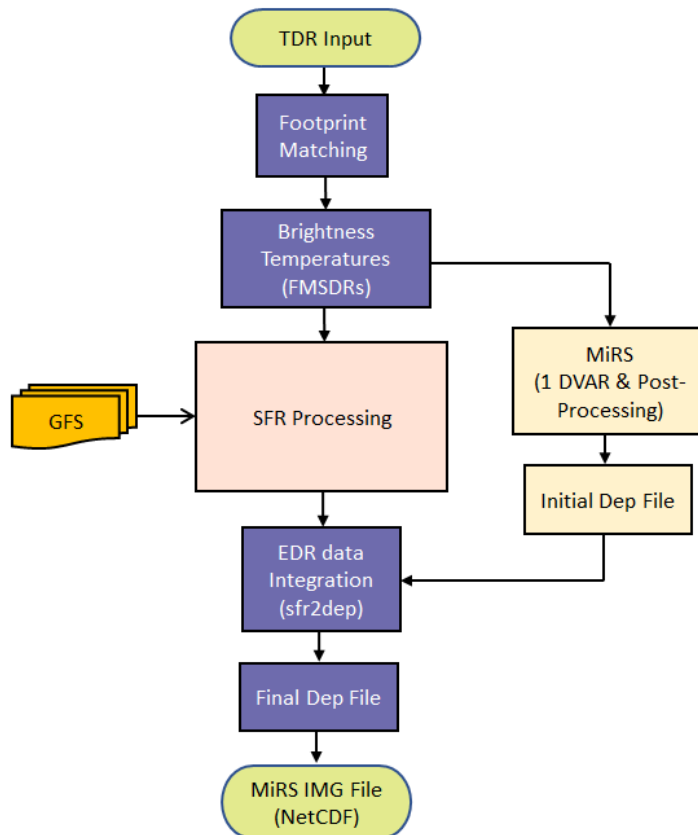


Figure 2-1. Diagram showing SFR processing as a sub-system within MiRS

MiRS processing starts with TDR ingestion and is followed by footprint matching for sensors with channels that have significantly different resolutions (MiRS ATBD Section 2.1). An intermediate binary FMSDR file contains the footprint-matched radiance and the associated geolocation data. It serves as the input to both the SFR processing and the MiRS 1DVAR. An output file (final dep) combines the SFR product resulting from the SFR processing and the EDRs generated from MiRS post-processing. Finally, this file is converted to netCDF4 format and is distributed as MiRS IMG file.

Figure 2-2 shows the SFR processing flowchart.

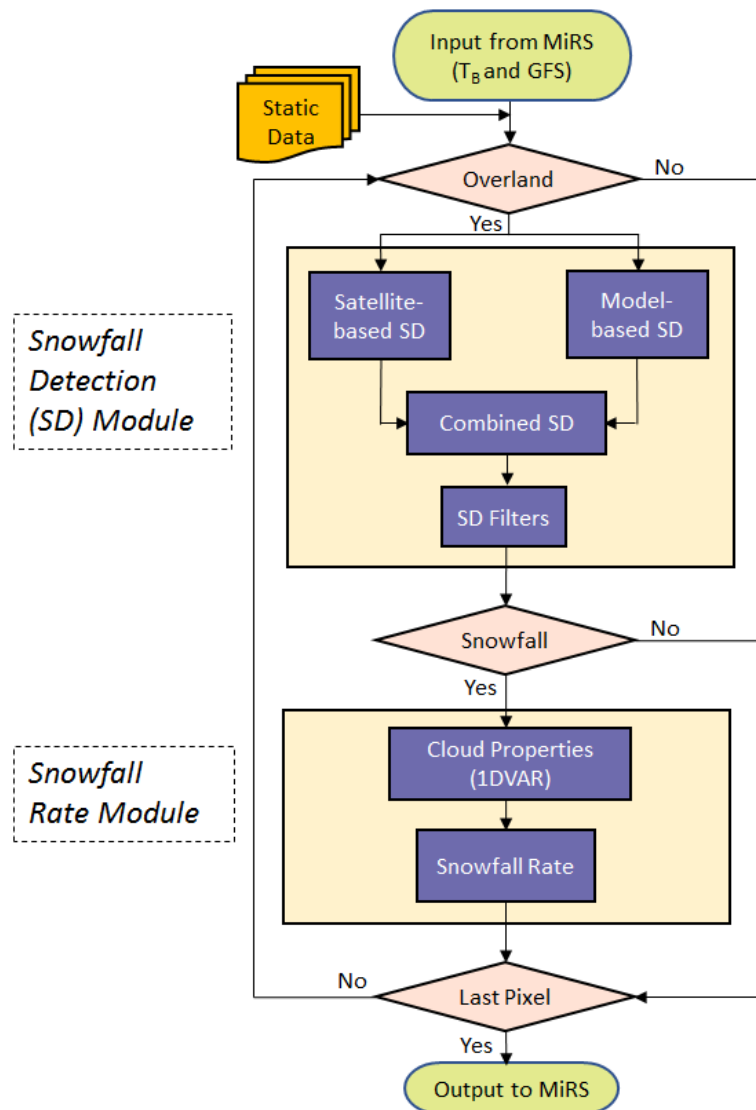


Figure 2-2. SFR processing flowchart

The SFR processing starts from an interface with the MiRS system where the MiRS intermediate FMSSDR data is ingested to the SFR sub-system. The input data also includes some static ancillary files and the Global Forecast System (GFS) model data produced by NOAA National Centers for Environmental Prediction (NCEP). The SFR algorithm consists of two components (algorithms): snowfall detection (SD) and snowfall rate. The two components are executed separately in two main modules (Fig. 2-2). The current algorithm only applies to over land while the satellite observations over ocean (including large inland lakes) and coast are flagged as undetermined. For an overland field-of-view (FOV), the processing first executes the SD module. The SD algorithm is composed of three main elements: a satellite-based SD element, a GFS model-based SD element, and a set of GFS model-based SD filters. The first two elements yield the probabilities of snowfall (POS) and are optimally combined to produce the final POS. If the POS passes the pre-defined thresholds and the SD filters are satisfied, snowfall is positively identified and the processing advances to the snowfall rate module. The SFR algorithm retrieves some cloud properties using a 1DVAR inversion method. The retrieved variables are then used to derive the final SFR. This process is performed for all FOVs in a satellite swath sequentially. Finally, the SFR output is combined with other MiRS non-sounding EDRs in the IMG netCDF4 file.

### **Inversion Processing**

Figure 2-3 describes the organization of the inversion 1DVAR process. The processing starts with the computation of first guesses of the control vector elements including some cloud properties. The first guesses are derived from brightness temperatures ( $T_{BS}$ ) and pre-derived empirical equations. An iteration scheme (Yan et al., 2008) follows in which  $T_{BS}$  are simulated with a forward operator (Weng et al., 2001) and the control vector in each cycle. Then the differences between the simulated and the observed  $T_{BS}$  ( $\Delta T_{BS}$ ) are checked against pre-set thresholds. The iteration terminates and the cloud properties from this cycle are retrieved if the simulation reaches convergence. Otherwise, the control vector is updated and iteration advances to the next cycle. The iterative loop also terminates if the convergence criterion is not met within five iterations.

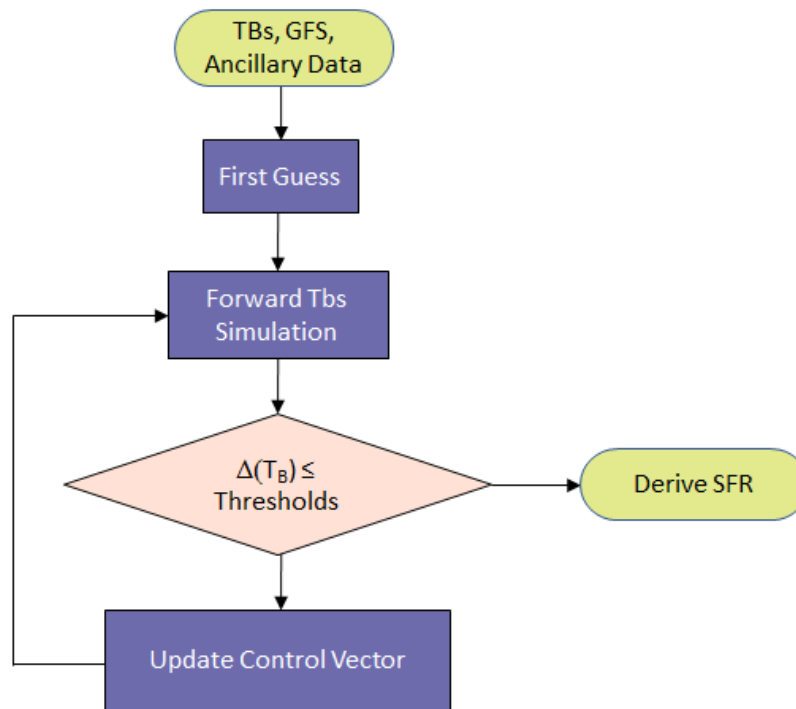


Figure 2-3. Diagram of inversion processing (1DVAR) to retrieve cloud properties for deriving SFR

## 2.2. Algorithm Input

Full description of the attributes of all input data used by the algorithm, including primary sensor data, ancillary data, forward models (e.g. radiative transfer models, optical models, or other model that relates sensor observables to geophysical phenomena) and look-up tables. Do not include file formats; these will be documented elsewhere. (*Document Object 14*)

**Writers:** Algorithm Scientists.

The SFR algorithm requires a number of data files to operate properly. The data files needed and their purpose are listed below.

**Input Data:** MiRS ATMS FMSDR data (single granule)

**Contents:** Footprint-matched radiometric measurements (brightness temperatures), and geolocation data.

**Format:** Binary

Number of Files: 1

Static/Dynamic: Dynamic

**Input Data:** Land-Sea Mask Data

Contents: Global surface type (land or ocean) data, 1/16 degree resolution

Format: Binary

Number of Files: 1

Static/Dynamic: Static

**Input Data:** Footprint Size Data

Contents: Footprint size to mask resolution ratio as a function of scan position. Data is required for determining surface type at each FOV.

Format: Ascii

Number of Files: 1

Static/Dynamic: Static

**Input Data:** SFR Limit Data

Contents: SFR upper and lower limits.

Format: Ascii

Number of Files: 1

Static/Dynamic: Static

**Input Data:** ATMS to MHS Measurement Conversion Coefficients

Contents: Coefficients to convert measurements from three ATMS channels, 88.2, 165.6, and 183.31±7 GHz to the MHS channels at 89.0, 157.0, and 191.31 GHz, respectively. The conversion is required to derive first guess for ice water path (IWP) because the original empirical equation was developed using the MHS measurements.

Format: Ascii

Number of Files: 1

Static/Dynamic: Static

**Input Data:** Cloud optical parameters

Contents: Look-up-table of three cloud optical parameters: optical depth, single-scattering albedo, and asymmetry factor calculated from Mie code. The LUT is used for radiative transfer calculations.

Format: Binary

Number of Files: 1

Static/Dynamic: Static

## 2.3. Theoretical Description

### 2.3.1. Physical Description

Comprehensively describe the sensor physics and the associated geophysical phenomenology key to the product retrieval. (*Document Object 15*)

**Writers:** Algorithm Scientists.

The Advanced Technology Microwave Sounder (ATMS), flown on the Suomi-NPP and JPSS satellites, is a cross-track scanner with 22 channels. Channel selection and frequencies are similar to the heritage AMSUA/MHS sensors flown on the NOAA and Metop polar-orbiting series of satellites. Channel frequencies are chosen to provide sounding of atmospheric temperature, water vapor and cloud, hydrometeors such as rain and ice water, as well as retrieval of surface characteristics. MiRS ATBD Table 2-1 summarizes the ATMS channels and passband characteristics, instrument noise, and beam widths. Furthermore, MiRS ATBD Figure 2-5 shows the ATMS atmospheric weighting functions for all 22 channels based on a U.S. Standard Atmosphere. The

weighting functions provide a synthesis of how the atmospheric state at each vertical layer (primarily through absorption/emission) contributes to the observed upwelling radiance at the top of the atmosphere for each channel. The SFR algorithm utilizes a combination of window and sounding channels, i.e. 23.8, 31.4, 53.6, and all frequencies at and above 88.2 GHz for snowfall detection and snowfall rate retrieval. The  $T_B$ s at high frequencies, including the water vapor sounding channels around 183.31 GHz, are usually lowered due to the scattering effect of ice particles in the presence of snowfall. Since the weighting functions of these frequencies peak at different levels of the atmosphere, the uncalibrated SFR represents snowfall from the precipitating layer. The retrieval is further calibrated with ground radar-based precipitation analyses so the SFR product is more representative of surface snowfall (Section A2.3). Figure 2-4 displays the modeled impact of cloud and hydrometeors on over-ocean brightness temperatures. The red line indicates  $T_B$  under the influence of cloud liquid water (CLW), graupel (GWP), and rain. The depressing effect of ice particles (graupel in this case) is significant at the ATMS high frequencies if one compares the red and the green lines. The latter is similar to the former minus the effect of graupel. The main physical foundation of the SFR algorithm is the  $T_B$  sensitivity to the effect of ice scattering.

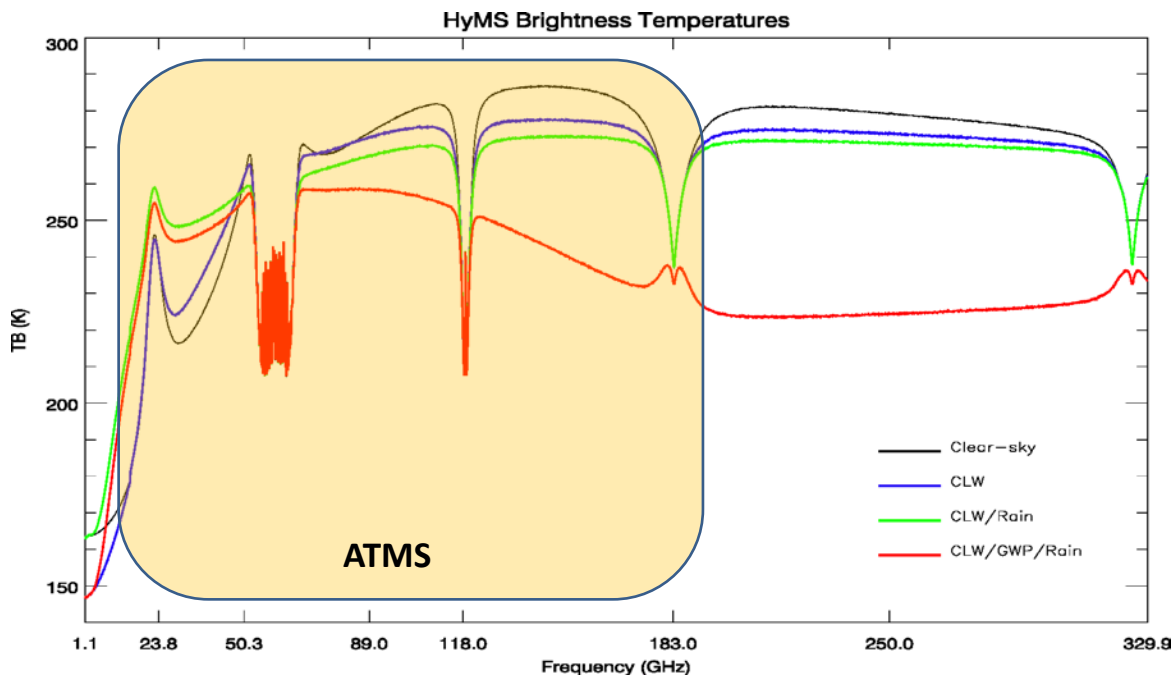


Figure 2-4. Impact of cloud ice and rain in simulated brightness temperatures in the range 1 to 330 GHz. The shaded area indicates the spectral range of the ATMS channels.

In addition to the impact of atmospheric conditions on upwelling radiances, surface characteristics also modulate observed radiances via changes in surface emissivity, which

can be highly variable and dependent on polarization, frequency, satellite zenith angle, and surface type. The SFR algorithm employs the two-stream radiative transfer model (RTM) developed by Yan et al. (2008) to retrieve cloud properties in a 1DVAR scheme. One of the major advantages of adopting the 1DVAR approach is that it simultaneously retrieves both cloud properties and emissivity. This ensures that all retrieved variables are physically consistent and reconcilable in the framework of the two-stream radiative transfer model. It also eliminates the need for a priori knowledge of the land surface types and their emissivity. The SFR algorithm is applicable to all land surfaces including snow cover.

### 2.3.2. Mathematical Description

Comprehensively describe the mathematics used by the algorithm, including all assumptions, simplifications, approximations. (*Document Object 16*)

**Writers:** Algorithm Scientists.

#### Snowfall Detection Algorithm

The SFR algorithm includes an embedded SD algorithm (Kongoli et al, 2015 and 2018) which consists of two statistical models based on satellite measurements and meteorological variable from GFS, respectively.

The satellite SD model is a scheme that combines principal component analysis (PCA) of seven ATMS high-frequency brightness temperature measurements with the logistic regression technique to compute the probability of snowfall. Logistic regression is used to estimate the probability of a binary outcome Y as an exponential continuous function of a set of predictor variables:

$$P = \frac{\exp(\beta_0 + \beta_1 X_1 + \beta_2 X_2 + \dots \beta_n X_n)}{1 + \exp(\beta_0 + \beta_1 X_1 + \beta_2 X_2 + \dots \beta_n X_n)} \quad (2-1)$$

where P is the probability of success of the binary variable Y, which in this case is the POS; X is the vector of independent variables, which in this case are brightness temperature measurements; and  $\beta$  is the vector of regression coefficients. The logarithm of the odds of Y called the logit can be expressed as linear combination of independent variables as in multiple regression:

$$\text{Logit}(P) = \text{Ln}\left(\frac{P}{1-P}\right) = \beta_0 + \beta_1 X_1 + \beta_2 X_2 + \dots \beta_n X_n \quad (2-2)$$

The inverse of the logit function is called the logistic function:

$$P = \frac{\exp(\beta)}{1 + \exp(\beta)} \quad (2-3)$$

where  $\beta$  is the logit function or the multiple linear regression term in equation (2-2). The fitting procedure consists in iteratively finding the set of regression coefficients using maximum likelihood estimation of the joint distribution of the response  $Y$ :

$$g(y_1, y_2, \dots, y_n) = \prod_{i=1}^n p_i^{y_i} (1 - p_i)^{1-y_i} \quad (2-4)$$

where  $y_i$  is an individual measured value of  $Y$ , e.g., arbitrarily assigned 1 for snowfall and 0 for no-precipitation, and  $p_i$  is the probability that  $y_i$  takes on the value of 1, e.g., for snowfall. Note that  $p_i$  is computed using equation (2-1). This differs from ordinary least squares regression where a unique analytic solution can be found in closed form.

One potential problem in applying logistic regression is the stability of regression coefficients when predictor variables are correlated. To address the problem of multicollinearity in predictor variables while retaining most of the information content, the seven-dimensional ATMS input data set is reduced to two or three uncorrelated principal components that retain most of the variance of the original data. In addition, the simple multivariate form in equations (A2-1) and (A2-2) would be preferable to more complex expressions, e.g., the power of predictor variables or other nonlinear terms, to achieve a solution more easily (Crosby et al., 1995). Another predictor variable considered (in addition to principal components) is the satellite local zenith angle. It is selected based on statistical significance results. The final satellite SD model has the following form:

$$\ln(P/(1 - P)) = a_0 + a_1*PC1 + a_2*PC2 + a_3*PC3 + a_4*\cos LZA \quad (2-5)$$

where  $\cos LZA$  is the cosine of the local zenith angle,  $PC1$ ,  $PC2$ , and  $PC3$  are the first three principal components computed from the seven-channel ATMS training data set, and  $a_0$ ,  $a_1$ ,  $a_2$ ,  $a_3$ , and  $a_4$  are the logistic regression coefficients computed from the training data set using maximum likelihood estimation.

ATMS observations at high frequencies exhibit different characteristics under warmer and colder conditions:  $T_B$ s are generally higher during snowfall than no-precipitation in colder weather while the opposite is true in warmer weather. This is a response of the water vapor sounding channels to the amount of water vapor in the atmosphere that is highly correlated to temperature. The satellite SD model is therefore divided into two temperature regimes based on the value of the temperature sounding channel at 53.6 GHz: warm regime (limb-corrected 53.6 GHz,  $244 \text{ K} < T_{B53L} \leq 252 \text{ K}$ ) and cold regime ( $240 \text{ K} \leq T_{B53L} \leq 244 \text{ K}$ ). The coefficients in Equation (2-5) are separately trained for the two regimes. FOVs with

T<sub>B</sub>53L lower than 240 K is flagged as no-retrieval, and those with T<sub>B</sub>53L greater than 252 K are considered no-snowfall (could be rainfall).

A similar probabilistic logistic regression approach was adopted for snowfall detection using forecast meteorological variables as predictors. Equations (2-1) ~ (2-4) also apply to this weather-based SD model except that the X vector is now composed of GFS forecasted cloud thickness, relative humidity from surface to 3-km above surface, and vertical velocities at 2 and 3 km.

The final POS is an optimal combination of the satellite-based and weather-based SD models:

$$P = W_s * P_s + W_w * P_w \quad (2-6)$$

where  $P$  refers to POS,  $W$  refers to the weight, and subscripts  $s$  and  $w$  refer to the satellite and the weather-based SD algorithms, respectively. Note that  $W_s + W_w = 1$ .

### Snowfall Rate Algorithm

The SFR algorithm (Meng et al., 2017; Ferraro et al., 2018) is based on the one dimensional variational retrieval (1DVAR) approach (Yan et al., 2008). A single-layer scattering-based RTM (Weng et al., 2001) is the forward operator utilized for TB simulation. The inversion is an iterative physical algorithm that optimally extracts the information content present in the measurements. Equation (2-7) explains the retrieval concept:

$$\begin{bmatrix} \Delta I_w \\ \Delta D_e \\ \Delta \varepsilon_{23} \\ \Delta \varepsilon_{31} \\ \Delta \varepsilon_{88} \\ \Delta \varepsilon_{165} \\ \Delta \varepsilon_{176} \end{bmatrix} = \left[ (A^T A + E)^{-1} A^T \right] \begin{bmatrix} \Delta T_{B23} \\ \Delta T_{B31} \\ \Delta T_{B88} \\ \Delta T_{B165} \\ \Delta T_{B176} \end{bmatrix} \quad (2-7)$$

where the control variables on the left are cloud ice water path  $I_w$ , ice particle effective diameter  $D_e$ , and emissivity  $\varepsilon$ ; Jacobian matrix  $A$  includes all partial derivatives of the simulated  $T_{BS}$  with respect to each of the control variables;  $E$  refers to the observation and background error matrix;  $\Delta T_B$  represents the difference between T<sub>B</sub> observations and RTM simulations; the  $\Delta$  of control variables indicates the difference between two consecutive iterations; and the number subscript refers to frequency. It is noted T<sub>B</sub> simulation also requires total precipitable water ( $TPW$ ), skin temperature ( $T_s$ ), and cloud temperature ( $T_e$ ).

The GFS forecasted  $TPW$  and  $T_s$  are utilized in the RTM and  $T_e$  is derived empirically from  $T_B$  observations. The control variables  $I_w$  and  $D_e$  are the targeted cloud properties to be retrieved from the 1DVAR. The mathematical solution to the inversion problem is to minimize the  $\Delta T_B$  matrix by varying the control variables at each iteration. The retrieved cloud properties are then utilized to derive ice water content (IWC). Furthermore, ice particle terminal velocity,  $V$ , is computed from a model developed by Heymsfield and Westbrook (2010). The product of IWC and  $V$  result in SFR:

$$SFR_u = A \int_0^\infty D^2 e^{-D/D_e} \left[ \left( 1 + BD^{3/2} \right)^{1/2} - 1 \right]^2 dD \quad (2-8)$$

$$A = \frac{I_w \eta \delta_0^2}{12 \rho_w \rho_a D_e^4} \quad (2-9)$$

$$B = \frac{8}{\eta \delta_0^2} \sqrt{\frac{g \rho_i \rho_a}{3 C_0}} \quad (2-10)$$

where  $D$  is the diameter of ice particle (assuming spherical habit),  $\eta$  is dynamic viscosity of air,  $\rho_w$  is water density,  $\rho_a$  is air density,  $\rho_i$  is ice density,  $\delta_0$  and  $C_0$  are fitting parameters,  $\delta_0 = 8.0$  and  $C_0 = 0.35$ . There is no analytical solution for Equations (2-8)-(2-10) so the equations are solved numerically using Romberg's method. An implicit assumption is made in the above equations, i.e., IWC is linearly distributed in the cloud column. Calibration was conducted against the National Stage IV quantitative precipitation estimates (QPE) product to statistically account for the deviation from the assumption. Stage IV is gauge corrected radar precipitation analyses produced by NCEP. The final SFR equation is derived through histogram matching (Kidder and Jones, 2007) between  $SFR_u$  and collocated Stage IV data:

$$SFR = a_1 SFR_u + a_2 SFR_u^2 + a_3 SFR_u^3 \quad (2-11)$$

where  $a_1 = 1.5813$ ,  $a_2 = -0.2236$ , and  $a_3 = 0.0216$ .

## 2.4. Algorithm Output

Describe the output data products - not format - at a level of detail to determine if the product meets user requirements. (*Document Object 17*)

**Writers:** Algorithm Scientists.

The output of the current SFR algorithm is the water equivalent instantaneous snowfall rate over global land. It is stored in the MiRS IMG netCDF4 output files.

## 2.5. Performance Estimates

### 2.5.1. Test Data Description

Description of data sets used for V&V, including unit tests and system test, either explicitly or by reference to the developer's test plans, if available. This will be updated during operations to describe test data for maintenance. (*Document Object 31*)

**Writers:** Development Testers

The ATMS SFR algorithm is validated and verified using three sets of data: the NCEP Stage IV, the Multi-Radar Multi-Sensor (MRMS) radar precipitation data produced by NOAA National Severe Storms Laboratory (NSSL), and the in-situ Snow Telemetry (SNOTEL) data produced by the Natural Resources Conservation Service (NRCS). The Stage IV data is hourly precipitation estimates on a 4-km grid covering CONUS except the Pacific Northwest. MRMS is instantaneous precipitation analyses over CONUS with a 0.01 degree resolution. SNOTEL is an automated system of snowpack and related climate sensors that collect data including hourly water equivalent snowfall accumulation. There are more than 700 SNOTEL stations in the Western US including Alaska, mostly in remote high mountains. The Stage IV and MRMS V&V data is from winter 2017-2018 while SNOTEL data is three winters from 2014-2017.

### 2.5.2. Sensor Effects

Characterize sensor effects that may contribute to retrieval error. Include the following effects if relevant:

- o Flowed-through effects of sensor noise (radiometric, thermal, or other) on the quality of products, using text and graphics (scatter plots, image displays, etc.).
- o Flowed-through effects of calibration errors (radiometric, including structured scenes and response versus scan, or any sensor biases) on the quality of products, using text and graphics.
- o Flowed-through spatial and spectral error effects (pointing and geolocation errors, apodization, modulation transfer function (MTF), point-spread function (PSF), out-of-band (OOB) response, near-field stray light, Earth shine, solar contamination, polarization, cross talk, etc.) on the quality of products, using text and graphics.
- o Flowed-through effects of un-modeled or neglected geophysical phenomena on the quality of products, using text and graphics.

(*Document Object 18*)

**Writers:** Algorithm Scientists.

The sensor-related errors are generally on the order of a degrees K or less. Errors of this magnitude can be expected to only have minor effect on SFR retrieval. Figure 2-5 presents the result of a  $T_B$  perturbation study on the S-NPP ATMS SFR. The 165.5 GHz and  $183.31 \pm 7$  GHz channels are used for this study because statistical analyses reveal that they have much larger impact on SFR than the other channels. Figure 2-5 shows that the effect of 1.5 K perturbation at the 165.5 GHz and up to 3 K perturbation at the  $183.31 \pm 7$  GHz only result in very small changes in SFR where less than 0.4 mm/hr variation is observed if SFR is up to 5 mm/hr.

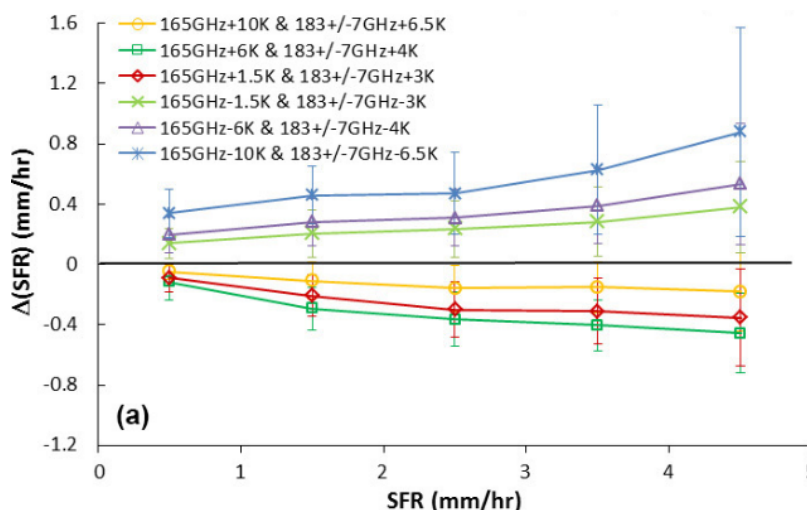


Figure 2-5. SFR change corresponding to TB perturbation at 165.5 GHz and  $183.31 \pm 7$  GHz

### 2.5.3. Retrieval Errors

Accuracy of products, as measured by V&V testing, and compared to accuracy requirements. Refer to relevant test reports. (*Document Object 39*)

**Writers:** Algorithm Scientists and Development Testers should collaborate

### Product Accuracy

The JPSS L1RD requirements for SD and SFR are given in Table 1-2. The SD and SFR algorithms were validated against in-situ data, radar and gauge corrected radar precipitation analyses. Product accuracy is determined from these validation studies.

The validation datasets utilized for SD validation are MRMS and the Quality Controlled Local Climatological Data (QCLCD) data available from NOAA National Centers for Environmental Information (NCEI). The latter is in-situ hourly snowfall accumulation collected by gauges throughout CONUS and Alaska. Three years (2015 – 2017) of

validation data are collocated with the S-NPP ATMS SFR (SD is embedded) and the validation metrics are computed including Accuracy Rate, Probability of Detection (POD), False Alarm Rate (FAR), Heidke Skill Score (HSS). Accuracy Rate is defined as the fraction of correct snowfall and no-snowfall retrieved. The statistics are determined separately for CONUS as Alaska as follows (Table 2-1):

Table 2-1. Over-Land SD Validation Metrics

Source/Coverage	Accuracy	POD	FAR	HSS
QCLCD/CONUS	0.88	0.51	0.08	0.40
QCLCD/Alaska	0.86	0.46	0.10	0.37
MRMS/CONUS	0.90	0.53	0.06	0.43

The SFR algorithm is validated against Stage IV and MRMS data over CONUS from winter 2016-2017. Figure 2-6 presents the scatter plot and the probability distribution (histogram) of the Stage IV-based validation. Table 2-2 lists the corresponding validation metrics. Figure 2-7 and Table 2-3 are similar to Figure 2-6 and Table 2-2, respectively, but for validation against MRMS.

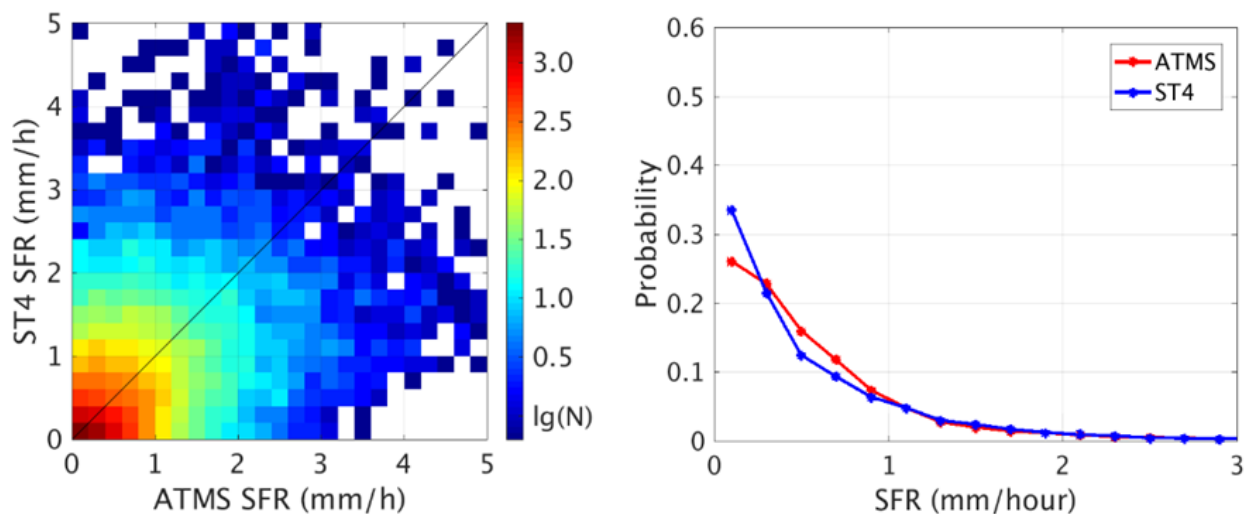


Figure 2-6. S-NPP ATMS SFR validation against Stage IV; left: scatter plot, right: probability distribution

Table 2-2. Over-Land SFR Validation Metrics against Stave IV over CONUS

Correlation Coefficient	Accuracy (mm/hr)	Precision (mm/hr)
0.50	0.06	0.74

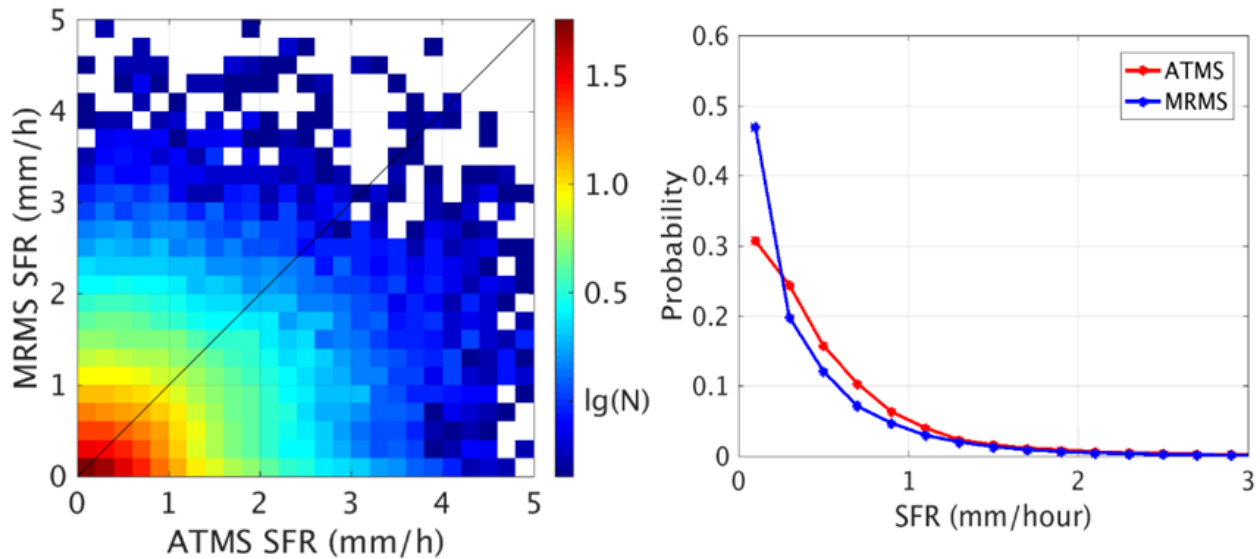


Figure 2-7. S-NPP ATMS SFR validation against Stage IV; left: scatter plot, right: probability distribution

Table 2-3. Over-Land SFR Validation Metrics against MRMS over CONUS

Correlation Coefficient	Accuracy (mm/hr)	Precision (mm/hr)
0.43	0.14	0.62

It is noted that both MRMS and Stage IV are derived from the NEXRAD radar reflectivity except that the latter is gauge corrected so is considered to have higher accuracy.

The validation results demonstrate that the SFR and the embedded SD meet the JPSS Threshold Requirements but some do not yet meet the Objective Requirements. The latter includes SFR precision and SD POD over Alaska.

**Error Budget**

Organize the various error estimates into an error budget, presented as a table. Error budget limitations should be explained. Describe prospects for overcoming error budget limitations with future maturation of the algorithm, test data, and error analysis methodology. (*Document Object 19*)

**Writers:** Algorithm Scientists.

Table 2-4 shows the error budget for the ATMS SFR algorithm.

Table 2-4. ATMS SFR Error Budget

Error Source	Magnitude of Retrieval Impacts	Mitigation Strategies
Sensor Noise	<ul style="list-style-type: none"> <li>• Less than 5%</li> </ul>	
Bias from GFS Model	<ul style="list-style-type: none"> <li>• Less than 5%</li> </ul>	
Sensor Bias	<ul style="list-style-type: none"> <li>• Less than 10%</li> </ul>	Current scan-dependent biases in ATMS SDRs are being investigated by cal/val team and if a physically-based mitigation approach is developed, the MiRS algorithm can easily switch from processing TDRs to SDRs. The SFR algorithm shares input data with MiRS so will switch input with MiRS.
Forward Model Bias	<ul style="list-style-type: none"> <li>• 10 - 40%</li> </ul>	<ul style="list-style-type: none"> <li>• Improve RTM assumptions such as expand the range of ice particle effective diameter in the LUT of cloud optical parameters , incorporate emission effect from supercooled cloud droplets, and adopt non-spherical ice particle shape etc.</li> <li>• Explore the possibility to employ MiRS retrieved cloud properties in the SFR algorithm</li> </ul>
First Guess Bias	<ul style="list-style-type: none"> <li>• Up to 50 - 75%</li> </ul>	Some first guess parameters are derived from a single empirical equation. These empirical relationships need to be stratified into several categories based on atmospheric and surface conditions.

## 2.6. Practical Considerations

### 2.6.1. Numerical Computation Considerations

Describe how the algorithm is numerically implemented, including possible issues with computationally intensive operations (e.g., large matrix inversions, truncation and rounding). (*Document Object 21*)

**Writers:** Development Programmers.

The ATMS SFR algorithm is programmed in C with the exception of the RTM which is programmed in Fortran-90. Double precision variables are defined where computation accuracy requires such precision. The SFR processing requires rather limited computation resources. The algorithm starts with the detection of snowfall utilizing the SD algorithm which is a statistical model and is very computationally efficient. Only if snowfall is detection will the 1DVAR-based SFR algorithm be executed. The forward model is a one-layer RTM which is also much more efficient than a multi-layer model such as CRTM.

## 2.6.2. Programming and Procedural Considerations

Describe any important programming and procedural aspects related to implementing the numerical model into operating code. (*Document Object 22*)

**Writers:** Development Programmers.

The AMSU/MHS SFR algorithm has been running in MiRS operationally for several years at NOAA. There are many similarities between the AMSU/MHS SFR processing and the ATMS SFR processing. The ATMS SFR code has been integrated in MiRS and fully tested for proper execution.

## 2.6.3. Quality Assessment and Diagnostics

Describe how the quality of the output products and the retrieval itself is assessed, documented, and any anomalies diagnosed. (*Document Object 23*)

**Writers:** Algorithm Scientists.

The SFR product is visually inspected for anomaly on the operational side at NOAA/NESDIS Office of Satellite and Product Operations (OSPO). The SFR development team at NOAA and CICS-University of Maryland also maintains a near real-time SFR website: <http://cics.umd.edu/sfr/>. The ATMS SFR product is monitored through the site and any anomaly is investigated and solutions are developed where it is feasible.

The SFR product is often assessed through comparisons with Stage IV and MRMS precipitation analyses in case studies for significant snowstorms. The product has also gone through several official assessments at NWS Weather Forecast Offices. More assessment will be conducted as the algorithm reaches higher level of matures in the future. The SFR team will also develop the capability to monitor SFR quality through routine comparisons with Stage IV and MRMS data.

## 2.6.4. Exception Handling

List the complete set of expected exceptions, and describes how they are identified, trapped, and handled. (*Document Object 24*)

**Writers:** Development Programmers.

The SFR processing takes ATMS input data from MiRS. Therefore, any exceptions caused by issues with the ATMS data will be handled through MiRS.

Checks are built in the SFR code to capture missing or erroneous GFS data. The SFR processing will exit in such case and the product flagged as missing.

## 2.7. Validation

Describe how the algorithm has been or should be validated at a level of detail appropriate for the current algorithm maturity. (*Document Object 26*)

**Writers:** Algorithm Scientists.

Refer to section 2.5.3 for the SFR validation studies.

---

### 3. ASSUMPTIONS AND LIMITATIONS

Figures used in Section 3 should be numbered Figure 3-1, Figure 3-2, etc.

Tables used in Section 3 should be numbered Table 3-1, Table 3-2, etc.

#### 3.1. Performance Assumptions

Describe all assumptions that have been made concerning the algorithm performance estimates. Note any limitations that apply to the algorithms (e.g., conditions where retrievals cannot be made or where performance may be significantly degraded. To the extent possible, the potential for degraded performance should be explored, along with mitigating strategies. (*Document Object 20*)

**Writers:** Algorithm Scientists.

Meng et al. (2017) examined the various assumptions made in the SFR algorithm and their impact on the algorithm performance. The assumptions relevant to the 1DAVR retrieval are constant ice particle mass density, exponential ice particle size distribution, and spherical ice particle shape. Among them, size distribution and shape play more important role in the retrieval accuracy than the mass density. Further study on the size distribution assumption and adopting non-spherical shape or aggregates will benefit the SFR algorithm.

The SFR algorithm is applicable if the following criterion is met:  $T_{B53L} \geq 240$  K. Analysis reveals that this condition is statistically equivalent to 2-m temperature ( $t_{2m}$ ) equals about -15 °C. This limitation results in flagged SFR in most of the interior Alaska and other high latitude regions in winter. In addition, SD performance is usually inferior if  $240$  K  $\leq T_{B53L} \leq 244$  K (equivalent to  $-15$  °C  $\leq t_{2m} \leq 6$  °C, i.e. cold regime) compared to  $244$  K  $< T_{B53L} \leq 252$  K (warm regime). Further study is required to improve SD performance in the cold regime and extend to even colder regions.

The RTM used to simulate  $T_{BS}$  only takes into consideration the scattering effect from ice particles but not the emission effect of supercooled cloud liquid droplets. This assumption results in SFR underestimation.

The current SFR algorithm only applies to over land. To meet the JPSS requirement for global SFR, development is required to extend the algorithm to over ocean including coast and sea ice.

### 3.2. Potential Improvements

Describe potential future enhancements to the algorithm, the limitations they will mitigate, and provide all possible and useful related information and links. (*Document Object 25*)

**Writers:** Algorithm Scientists.

The SFR algorithm can benefit from development in several areas as described below.

#### Ice Particle Shape

The SFR algorithm assumes spherical shape ice particles. The LUT of cloud optical parameters is constructed from Mie's theory based on this assumption. However, ice particles in real world are non-spherical and often exist as aggregates. There have been some studies on the scattering properties of more realistic ice particle shapes (Liu 2004; Kuo et al., 2016). A study on the MHS SFR has shown that the assumption of non-spherical shape ice particles may lead to improved SFR accuracy (Meng, et al., 2017).

#### First Guess IWP (stratify)

A single empirical equation is used to derive first guess IWP from  $T_B$ . This approach has been proven inadequate. Multiple equations will need to be developed stratified by environmental conditions and satellite measurements. This task has the potential to significantly improve the SFR estimates.

#### Emission from Supercooled Cloud Droplets

The RTM used for  $T_B$  simulation does not take into consideration the emission effect from supercooled cloud droplets and causes SFR to underestimate when there is abundance of such droplets, e.g. strong convective snowstorm or coastal environment. The RTM should be modified to include the emission effect of cloud droplets or CLW. This effort requires the development of an approach to determine first guess CLW. It is an important but challenging task. However, incorporating CLW in the RTM is critical to the improvement of SFR in the Alaska region and also to the development of ocean SFR in the future.

#### Alaska SFR

Alaska has a stronger demand for polar-orbiting satellite products than CONUS because it has limited radar and GEO satellites coverage. However, Alaska has very different climate than most CONUS which can lead to degraded performance for SFR. The feedback from product assessment at Alaska WFOs reveals that SFR underestimation is a common issue in Alaska southeast and the Anchorage region. The SD filters also require further adjustment due to the unique meteorological conditions prevailing in this region. In addition,

the interior Alaska is flagged as too-cold by the current SFR algorithm in most winter season. A SD cold-extension algorithm is required to extend the current algorithm to colder conditions. An Alaska-specific SFR algorithm will improve SFR performance considerably for this region.

## **Ocean/Coast/Sea Ice SFR**

The current SFR is an over-land product. There is a significant user demand for snowfall information over ocean including over coast and sea ice. The JPSS L1RD also requires SFR to have global coverage. Ocean/coast/sea ice SFR algorithms can be developed following similar framework as land SFR. Due to the different dominant snowfall mode over land and over ocean, however, the development of ocean/coast/sea ice SFR algorithms is expected to be a very challenging task.

## **Utilizing MiRS Retrievals**

MiRS produces a comprehensive suite of EDR products through a 1DVAR retrieval algorithm and post-processing. These products can be explored for their potential to enhance SFR retrieval. For instance, the MiRS temperature and water vapor profiles might replace the GFS forecast variables in the SFR algorithm if the quality of the MiRS products is comparable or superior to the GFS counterparts. Another MiRS retrieval that holds potential to improve SFR is the graupel water path (GWP). This variable is closely related to IWP and might serve as the first guess IWP or even replace the retrieved IWP in the SFR algorithm. It is noted that MiRS GWP is not yet an operational product over snow cover. Therefore, focused study is necessary to examine the validity of its application in SFR enhancement.

---

## 1. REFERENCES

- Crosby, D. S., R. R. Ferraro, and H. Wu, 1995. Estimating the probability of rain in an SSM/I FOV using logistic regression, *J. Appl. Meteorol.*, 34, 2476–2480.
- Heymsfield, A. J., and C. D. Westbrook (2010), Advances in the estimation of ice particle fall speeds using laboratory and field measurements, *J. Atmos. Sci.*, 67(8), 2469–2482, doi:10.1175/2010JAS3379.1.
- Kidder, S. Q., and A. S. Jones (2007), A blended satellite total precipitable water product for operational forecasting, *J. Atmos. Ocean. Technol.*, 24(1), 74–81, doi:10.1175/JTECH1960.1.
- Kongoli, C., H. Meng, J. Dong and R. Ferraro, 2018. A Hybrid snowfall detection method from satellite passive microwave measurements and global weather forecast models, *Quarterly Journal of Royal meteorological Society*, DOI:10.2002/qj3270.
- Kongoli, C., H. Meng, J. Dong and R. Ferraro. 2015. A Snowfall detection algorithm over land utilizing high-frequency passive microwave measurements – Application to ATMS. *J. Geophys. Res. – Atmospheres*, 120(5), 1918–1932. DOI: 10.1002/2014JD022427.
- Kuo, K.-S., W. S. Olson, B. T. Johnson, M. Grecu, L. Tian, T. L. Clune, B. H. van Aartsen, A. J. Heymsfield, L. Liaos, and R. Meneghini (2016), The microwave radiative properties of falling snow derived from nonspherical ice particle models. Part I: An extensive database of simulated pristine crystals and aggregate particles, and their scattering properties, *J. Appl. Meteorol. Climatol.*, 55(3), 691–708, doi:10.1175/JAMC-D-15-0130.1.
- Liu, G. (2004), Approximation of single scattering properties of ice and snow particles for high microwave frequencies, *J. Atmos. Sci.*, 61(20), 2441–2456, doi:10.1175/1520-0469(2004)061<2441:AOSPO>2.0.CO;2.
- Meng, H., J., Dong, R., Ferraro, B., Yan, L., Zhao, C., Kongoli, N.-Y., Wang, and B., Zavodsky (2017), A 1DVAR-based snowfall rate retrieval algorithm for passive microwave radiometers, *J. Geophys. Res. Atmos.*, 122, doi:10.1002/2016JD026325.
- Ralph Ferraro, Huan Meng, Brad Zavodsky, Sheldon Kusselson, Deirdre Kann, Brian Guyer, Aaron Jacobs, Sarah Perfater, Michael Folmer, Jun Dong, Cezar Kongoli, Banghua Yan, Nai-Yu Wang, and Limin Zhao, 2018. Snowfall rates from satellite data help weather forecasters, *Eos*, 99, <https://doi.org/10.1029/2018EO096715>.
- Weng, F., B. Yan, and N. Grody (2001), A microwave land emissivity model, *J. Geophys. Res.*, 106, 20,115–20,123, doi:10.1029/2001JD900019.
- Yan, B., F. Weng, and H. Meng (2008), Retrieval of snow surface microwave emissivity from the advanced microwave sounding unit, *J. Geophys. Res.*, 113, D19206, doi:10.1029/2007JD009559.
-

END OF DOCUMENT